On the fatigue damage micromechanisms in Si-solution–strengthened spheroidal graphite cast iron

Sujakhu, Surendra; Castagne, Sylvie; Sakaguchi, M.; Kasvayee, K. A.; Ghassemali, E.; Jarfors, A. E. W.; Wang, W.

2017

Sujakhu, S., Castagne, S., Sakaguchi, M., Kasvayee, K. A., Ghassemali, E., Jarfors, A. E. W., et al. (2017). On the fatigue damage micromechanisms in Si-solution–strengthened spheroidal graphite cast iron. Fatigue & Fracture of Engineering Materials & Structures, in press.

https://hdl.handle.net/10356/85822

https://doi.org/10.1111/ffe.12723

On the fatigue damage micromechanisms in Si-solution-strengthened spheroidal graphite cast iron

S. Sujakhu[1], S. Castagne[1], M. Sakaguchi[2], K.A. Kasvayee[3], E. Ghassemali[3], A.E.W. Jarfors[3], W. Wang[4]

[1]School of Mechanical and Aerospace Engineering, Nanyang Technological University, Singapore, 639798, [2]Department of Mechanical Engineering, Tokyo Institute of Technology, Tokyo 152-8552, Japan, [3]School of Engineering, Jönköping University, Box 1026, SE-551 11 Jönköping, Sweden, [4] Advance Remanufacturing and Technology Centre, Singapore 637143

ABSTRACT

Graphite nodules in Spheroidal graphite cast iron (SGI) play a vital role in fatigue crack initiation and propagation. The graphite nodule growth morphology can go through transitions to form degenerated graphite nodules other than spheroidal graphite nodules in SGI microstructure. These graphite nodules significantly influence damage micromechanisms on SGI and could act differently. Most of the damage mechanism studies on SGI were focused on the role of spheroidal graphite nodules on the stable crack propagation region. The roles of degenerated graphite nodules on SGI damage mechanisms were not frequently studied. In this work, fatigue crack initiation and propagation tests were conducted on EN-GJS-500-14 and observed under SEM to understand damage mechanisms of different graphite forms. Crack initiation tests showed dominant influence of degenerated graphite nodules where early cracks initiated in the microstructure. Most of the spheroidal graphite nodules were unaffected at the early crack initiation stage; some of them showed decohesion from the ferrite matrix and internal cracking. At the crack propagation region, graphite-ferrite matrix decohesion was the frequent damage mechanism observed with noticeable crack branching around graphite nodules and the crack passing through degenerated graphite nodules. Finally, graphite nodules after decohesion acted like voids which grew and coalesced to form microcracks eventually causing rapid fracture of the remaining section.

Keywords spheroidal graphite cast iron; damage micromechanisms, fatigue crack initiation, fatigue crack propagation

NOMENCLATURE

a = crack length
A = area of graphite particle
A_m = area of circle of diameter equivalent to the maximum axis length of the graphite nodule

C_A = graphite growth due to reduced C solubility in austenite grain
C_E = graphite growth from eutectic solidification
C_F = graphite growth by euctoid transformation into ferrite
C_M = graphite nucleation and growth from melt
C_{eq} = carbon equivalent
$C(T)$ = compact type specimen
da/dN = crack growth rate
FCP = Fatigue Crack Propagation
l_m = maximum length of the graphite particle
N = fatigue load cycles
N_f = fatigue life to failure
OM = Optical microscope
R = fatigue load ratio
RSF = Roundness Shape Factor
SGI = Spheroidal Graphite cast Iron
SEM = Scanning Electron Microscope
UTS = Ultimate Tensile Strength
ΔK = stress intensity factor range
ΔK_{Start} = starting stress intensity factor range

Correspondence: S. Sujakhu. E-mail: surendra003@e.ntu.edu.sg

INTRODUCTION

In general, cast irons are viewed as brittle iron-carbon alloys. Spheroidal graphite cast iron (SGI) also known as ductile cast iron or nodular graphite iron, is indifferent from other cast irons in terms of graphite nodules. SGI have graphite nodules in the form of spheroid instead of flake as in the case of gray cast iron. The spheroidal graphite nodules allow SGI to have cast iron properties of good castability and economy with additional properties of higher fatigue resistance, toughness and ductility similar to those of carbon steel.[1] The matrix controls mechanical properties of SGI[1,3] and is used to designate different grades of SGI.[4] Ferritic SGI is characterised by good ductility and toughness whereas pearlitic SGI shows higher strength and better wear resistance with reduced ductility and impact resistance. Ferritic-pearlitic grades are the common SGI with intermediate properties between ferritic and pearlitic grade. Austempered SGI obtained after austempering heat treatment exhibits high strength, ductility and toughness similar to that of carbon steel.[5] With a wide range of properties, SGI have found applications in various forms; ductile iron pipes for transportation of water, sewage, slurries and processed chemicals; automobile components like crankshaft, gears, suspensions, brake; and as a storage container for nuclear waste.[4]

Graphite nodules in SGI not only influence mechanical properties, but also play a vital role in fatigue crack initiation and propagation. Iacoviello et al.[6] have summarised graphite nodules as: 'rigid spheres' not bonded to the matrix and acting like voids, 'crack arresters' that minimised the stress intensification at the crack tip, and 'crack closure effect riser'. Many studies[2,5-15] have been reported to investigate the fatigue mechanism and the influence of graphite nodules. Most of them had described graphite nodule-matrix decohesion as one of the most frequent damaging micromechanism in SGI materials. Studies[2,3,5,10,16] had shown the evident influence of the matrix microstructure and chemical composition on the fatigue resistance of SGI. Effect of stress ratio (R) and matrix microstructure on crack propagation resistance has been studied by Iacoviello et al.[2], who showed increasing crack growth rate with higher R. Kasvayee et al. studied microcrack initiation mechanism in high silicon cast iron during tensile loading[17] and microstructural strain distribution to explain crack initiation in SGI.[18] Shirani et al.[19] and Endo et al.[20] studied the effect of casting defects, indicating it as a common damage initiation point in cast material.

In-situ tensile tests with SEM studies are frequently used methods to investigate damage mechanisms. Damage mechanisms studies on ferritic SGI[2,7,8] stated that ferrite matrix-nodule was not necessarily a preferential crack path: in fact, the crack could propagate both nearby graphite nodules or by graphite nodule decohesion. Some secondary cracks were also reported, initiating both at the matrix-nodule interface and ferrite matrix. Similar studies on pearlitic SGI[2,6,21] indicated that fatigue crack grew along ferrite lamella either by delamination or in a transgranular mechanism with less frequent secondary cracks. Pearlite matrix-nodule decohesion was reported with internal cracking of graphite nodule into nodule core and nodule shield. Ferritic-pearlitic SGI crack path was characterized by the presence of many secondary cracks and clear graphite-matrix decohesion.[2,13] A study by Greno et al.[5] on austempered SGI described crack propagation by connecting small cracks emanating from nodules and their growth towards a principal crack.

Ferritic grades have good ductility and toughness whereas pearlitic grades have higher strength and wear resistance. To obtain combined properties, ferritic-pearlitic grades like EN-GJS-500-7 are considered in many applications. At higher Si content, casting solidification led to the formation of EN-GJS-500-14 with complete ferrite matrix. Silicon has a matrix strengthening effect on SGI, which also reduces variation of mechanical properties. [23] GJS-500-14 has a strength similar to that of GJS-500-7 with a higher ductility. Such high Si SGIs are capable of replacing higher strength SGI grades, and even some steels. Alhussein et al.[24] investigated the influence of Si content on the mechanical behaviour of ferritic SGI. Out of the investigated materials, GJS-500-14 showed promising results with significant increase in strength and less reduction in ductility. Understanding

the influence of graphite nodule on fatigue micromechanisms on the high Si SGI is crucial, as its use is extending to many automobile and wind turbine parts.

Shape and form of graphite nodule have significant effects on crack initiation and propagation behaviour of SGI. Even if SGI are treated to form spheroidal graphite nodules, other forms of graphite particles may grow due to the effect of other trace elements, or insufficient addition of inoculant or nodulizer during the solidification process.[25,26] Chunky, compacted, vermicular and irregular graphite nodules are commonly observed degenerated graphite nodules due to poor treatment of the melt. Other elements like S, F, O, P, N, B can be found in trace quantity in cast irons. These trace elements in the melt affect graphite nucleation and growth morphology.[26] The effect of these trace elements was divided into three parts; S and B as flake graphite stabilizer; O and F stabilising compacted or vermicular graphite growth; P and N mostly neutral. . It was reported that the graphite growth morphology was related to the impurities in the Fe-based liquid.[27] Inoculant and nodulizer are added into the melt to stabilize these trace elements and achieve desired graphite growth morphology. In SGI, inoculant is added to form micro-particles mostly oxides and sulphides that provide graphite nucleation sites. Skaland[28] reported that oxide and sulphide particles have at least one lattice space matching graphite lattice space to assist graphite nucleation and growth. It was also reported that MgO particles were found at the centre of graphite nodules.[25,29] The melt is treated with Mg-based nodulizer to control oxides and sulphides particles and favor spheroidal graphite growth. Mg forms MgO and MgS by dissolving O and S in the melt. Studies reported easy incorporation of atoms in the a-direction (basal plane in graphite hpc crystal structure) but with the lower probability of attaching in the c-direction [0 0 0 1] normal to the graphene monolayer.[27] Reported graphite growth direction was along a-direction for flake graphite nodule and along c-direction for nodular graphite. Compacted or vermicular graphite nodules grew in a complex way and did not have one preferred growth direction. Muhmond et al.[25] have shown that the graphite growth was along the circumference in SGI and the tentative size of different growth region was reported elsewhere.[7] These different growth regions created property variation within graphite nodules, which caused internal cracking of the graphite nodules at the interface of different growth regions.[22] Graphite form and its growth morphology have considerable influence on SGI damage mechanisms. So, it is important to include graphite growth morphology in damage mechanism studies.

In this study, the focus is on high Si EN-GJS-500-14. The aim of this work is to develop a comprehensive understanding of fatigue damage micromechanisms and the influence of graphite form and its growth morphology in different fatigue stages. Fatigue crack initiation (FCI) and fatigue crack propagation (FCP) tests

were conducted on miniature tensile and compact tension specimens, which were studied in SEM to observe the crack path and fracture surface. Base on the observed crack initiation and propagation results, fatigue damage mechanisms are proposed.

MATERIAL

EN-GJS-500-14, a ferritic spheroidal graphite cast iron (SGI) with chemical composition presented in Table 1 was used in this work. The sample material was casted as a 50 mm thick plate. To increase homogeneous graphite nucleation sites, inoculation process was performed both in ladle and in stream using commercially available inoculant *Foundrisil 67* (64 - 70 % Si, < 1.25 % Al, 0.17 – 1.25 % Ca, 0.75 – 1.25 % Ba and Fe balance). To favor spheroidal graphite growth morphology, Mg treatment was performed using commercially available Ce free FeSiMg nodulizer *Ceriumfritt* (44 - 48 % Si, 5.5 – 6.5 % Mg, < 0.1 % RE, 0.3 – 0.5 % Ca, < 0.7 % Al, < 0.05 % Ce and Fe balance). The combination of inoculation and Mg treatment process was adequate to produce a majority of spheroidal graphite nodules, but some fraction of graphite nodules were irregular and compacted as shown in Fig. 1. The tensile properties of the cast material are presented in Table 2. These properties are comparable with EN-GJS-500-7 which has a ferritic-pearlitic matrix. Microstructure characterization was based on image processing and ASTM standard E2567 was used to evaluate graphite morphology (size, nodularity and nodule count). To evaluate nodularity of the graphite nodules, roundness shape factor (RSF) was defined as shown in Fig. 2 and calculated by eq. (1). Average nodularity of the graphite nodules was evaluated based on area fraction using eq. (2), where graphite nodules were considered nodular if RSF is greater than 0.6. Around 122 graphite nodules of average diameter 27 µm were observed per mm^2 with an average % nodularity of 74 % as listed in Table 3.

Table 1 Chemical composition of EN-GJS-500-14 (%wt.)

C	Si	Cu	Mn	S	Mg	Sb	Fe	C_{eq}*
3.2	3.71	0.053	0.182	0.006	0.042	0.0058	92.5	4.15

* C_{eq} is carbon equivalent value that represents the equivalent percentage of carbon considering the effect of other alloying elements. Carbon equivalent mostly depends on C, Si and P content and can be calculated using C_{eq} = C% + 1/3(Si% + P%).

Table 2 Tensile properties of EN-GJS-500-14 (50 mm thick plate)

Young's modulus (GPa)	Yield Strength (MPa)	UTS (MPa)	Elongation to fracture (%)
170 ± 1	410 ± 9	511 ± 6	17 ± 6

Fig. 1 Microstructure of EN-GJS-500-14

Fig. 2 Roundness shape factor definition

Table 3 Microstructure characterization of EN-GJS-500-14 cast

Avg. Diameter (µm)	Nodularity by area (%)	Nodule count (per mm^2)	Pearlite fraction (%)	Graphite fraction (%)
27 ± 8	74 ± 3	122 ± 36	1 ± 1	9 ± 0.5

$$RSF = \frac{A}{A_m} = \frac{4\,A}{\pi\, l_m^2} \tag{1}$$

where, l_m is the maximum length of the graphite particle, A_m represents the area of a circle of diameter equivalent to the maximum axis length of the graphite particle and A stands for area of graphite particle.

$$\%\ Nodularity\ by\ area = \left(\frac{Area\ of\ all\ particles\ with\ RSF > 0.6}{Area\ of\ all\ graphite\ particles}\right)100 \tag{2}$$

Only graphite nodules with major axis diameter greater than 10 µm were considered as graphite nodules.

EXPERIMENTAL METHODS

Separate fatigue crack initiation (FCI) and fatigue crack propagation (FCP) tests were conducted on miniature specimens that could be easily loaded in SEM. Specimens were metallographically polished before the test, so that they can be observed in SEM without any preparation after the test. Both tests were load controlled and conducted on a Shimadzu ADT - AV10K1S5 air-servo system at a frequency of 10 Hz. Specimens for both tests were cut from same cast block to achieve similar crack growth direction. The details of specimens and experimental procedure for each test are described in the next sections.

Fatigue crack initiation test

For FCI tests, a miniature pin-loaded tensile test specimen was designed considering ASTM standard E8. Fig. 3 illustrates the design and dimensions of the specimen. Pin-loaded design was chosen as it was easier to align specimens and avoid biaxial stresses. To ensure failure at the gauge section, stress distribution was checked by FE simulation. Some iterations were done for the gauge section width and pin hole to finalize the best design. To remove stress concentration at the pin holes, a modified fixture as shown in Fig. 4 was designed

to clamp the specimen after aligning it on the pins. The modified fixture eliminates stress concentration at the pin hole and ensures uniform stress and failure at the gauge section.

Fig. 3 Miniature pin-loaded tensile specimen for crack initiation test (all dimensions in mm)

Fig. 4 Clamping fixture design for crack initiation test

ASTM standard E466 was referred to for the FCI tests. Constant amplitude fatigue tests were conducted at a load ratio (R) of 0.1 and maximum stress of 70% of the UTS, to ensure faster crack initiation. Crack initiation tests were aimed to identify possible initiation sites and to understand the influence of graphite nodules and their morphology. Tests were stopped after 200,000 load cycles for first crack initiation study. Tests were further continued to additional load cycles of 50,000, 30,000 and 20,000 for additional crack initiation and slow crack growth studies under OM and SEM.

Fatigue crack propagation test

The miniature compact specimen C(T), was designed considering ASTM standard E647 as shown in Fig. 5 for FCP tests. ASTM standard E647 provides a comprehensive guideline for the FCP test. C(T) specimens were metallographically polished before the test for clear visualisation of cracks. A load ratio of R = 0.1 was selected and initial stress intensity factor range (ΔK_{start}) of 13 $MPa\sqrt{m}$ was used based on FCP test results reported in previous work.[30] For the FCP study, two intermediate crack sizes were considered; one test stopped when the crack tip was still in the stable crack region and another one stopped as the crack tip approached the unstable region. Cracks on both surfaces of C(T) specimens were studied under the SEM. An additional specimen was tested to complete failure to study the role of graphite nodule at different fatigue stages along and near the crack path. Fracture surface studies of the failed C(T) specimen illustrated the fracture pattern and the role of graphite nodules at different fatigue stages. Finally, the crack initiation and propagation results were combined together to have a complete fatigue damage understanding of SGI microstructure.

Fig. 5 Miniature C(T) specimen design for crack propagation test (all dimensions in mm)

EXPERIMENTAL RESULTS

Fatigue crack initiation test

Samples were observed under SEM and OM for crack initiation stiudies. OM observation after 250,000 cycles showed initiation of crack in SGI microstructure for the applied loading conditions. Samples were further

tested and observed in between the tests to study crack initiation and growth. After around 400,000 cycles, most of the specimens showed multiple microcrack initiation. Detailed SEM studies were performed at different intervals and the observed damage initiation mechanisms are illustrated in Fig. 6 to Fig. 10. Damage initiation mechanisms can be explained in three types based on the point of crack initiation in the microstructure.

Fig. 6 Fatigue damage initiations on face 1 of the miniature FCI specimen(R = 0.1, S_{max} = 350 MPa, N = 390,000 cycles)

Fig. 7 Fatigue damage initiations on face 2 of the miniature FCI specimen(R = 0.1, Smax = 350 MPa, N = 390,000 cycles)

Firstly, cracks were initiated from degenerated graphite nodules. In Fig. 6: a) – d) and Fig. 7: a) – c), cracks were initiated earlier from compacted or irregular type graphite nodules. The occurrences of these degenerated graphite nodules were found to be vulnerable from the point of crack initiation, as those graphite nodules initiated early microcracks. Crack initiation in these graphite nodules were either by internal cracking of graphite nodule followed by crack growth into the matrix (Fig. 6: b, c, k, m and Fig. 7: c, e, f, l), or by decohesion followed by crack initiation from the interface (Fig. 6: d, e, f, o and Fig. 7: a, g, j, n), or by the combination of these mechanisms (Fig. 7: p, q). Graphite nodules with their major axis perpendicular to the loading direction were preferred initiation sites. The initiated cracks grew perpendicular to the loading direction and one of these initiated cracks grew as the main crack that led to final failure of the specimen. Other initiated cracks opened up on final failure (Fig. 8), which clearly illustrates internal cracking of the degenerated graphite nodules. It should be noted that all the initiated cracks did not show significant growth after the main crack started to grow.

Secondly, internal cracking of spheroidal graphite nodules into onion-like damage were observed. Similar results were also reported by Di Cocco et al.[8] for the in-situ tensile test. As shown in Fig. 6: g) – j) and Fig. 7: d), h), m), larger graphite nodules tend to internally crack into graphite core and shield. Not all nodular graphite showed such internal cracking; many were still intact in the ferrite matrix. Comparing the size of graphite nodules, it can be assumed that those larger nodules might have nucleated earlier in solidification stage, grown from the melt and then by diffusion of carbon from austenite; causing property difference within each graphite nodule. The resulting property difference inside the graphite nodule had caused internal cracking of fully grown spheroidal graphite nodules. Decohesion of graphite/matrix interface was reported as one of the common damage mechanism in SGI microstructure. Overall, graphite/matrix decohesion played an important role (Fig.

9), but at the point of cracks initiation from degenerated graphite nodules, most of the spheroidal graphite nodules did not initiated cracks even they were debond from the ferrite matrix. So, graphite/matrix decohesion was not necessarily the influencing mechanism at early crack initiation, but it was one of the important mechanisms in crack propagation. On few occasions, cracks were also initiated from graphite/ferrite interface (Fig. 6: l, q and Fig. 7: o). Such crack initiation was uncommon and mostly the spheroidal graphite nodules were intact in the ferrite matrix at the early crack initiation stage when the compacted and irregular graphite nodules already showed sign of initiation.

Lastly, crack initiations were also observed from shrinkage porosities present in the microstructure (Fig. 6: n and Fig. 7: i, k). Casting defects like shrinkage porosity have been reported as one of the major cause of early cracks initiation in cast irons.[19,20] The casting process for investigated SGI was optimized, so no larger casting defects were observed, only shrinkages porosities of a size comparable to graphite nodule were observed occasionally. These shrinkage porosities showed crack initiation at similar fatigue cycles as for the compacted graphite nodules. Shrinkage porosities were void in the matrix that gave stress concentration effect and cracks initiated earlier at the edge of the void. Only few such defects were observed in entire gauge section, the presence of which could initiate early crack depending on the size of the shrinkage defect.

Fig. 7 Degenerated graphites and initiated cracks after final failure of the specimen ($R = 0.1$, $S_{max} = 350$ MPa, $N_f = 474047$)

Fig. 8 Spheroidal graphite nodules after final failure of the specimen ($R = 0.1$, $S_{max} = 350$ MPa, $N_f = 474047$)

Fig. 9 Large irregular graphites on the fracture surface of the specimen ($R = 0.1$, $S_{max} = 350$ MPa, $N_f = 474047$)

After the crack initiation observations, the specimen was further tested to final failure. The crack in Fig. 6: b) on face 1 and Fig. 7: q) on face 2 propagated to form the main crack, which grew by connecting initiated cracks and debonded graphite nodules. Soon after the main crack started to grow, the specimen fractured and could not provide details on propagation mechanisms. Therefore, to clearly understand crack propagation micromechanisms separate FCP tests were conducted on miniature C(T) specimens. From the crack initiation study, it was difficult to predict which crack among those initiated would result into final failure, but it could be conjectured that one of the cracks initiated from larger defect (casting defects or degenerated graphite nodules) would further propagate. Fig. 6 and 7 also indicate roundness shape factor (RSF) for the graphite nodules initiating damage. Mostly the graphite nodules with lower RSF values initiate early cracks whereas the graphite nodules with RSF values higher than 0.9 showed internal cracking and decohesion mechanisms. Fig. 8 and 9

show the state of the graphite nodules after final failure. Quantitative analysis of damage initiation was reported in previous study.[31] Results showed that graphite nodule decohesion was dominant mechanism for spheroidal graphite nodules, whereas compacted graphite nodules initiated cracks mostly by combined decohesion and internal cracking. Cracks that initiated in compacted graphite nodules opened up without significant growth in crack size (Fig. 8). Spheroidal graphite particles (Fig. 9) after final failure shows an increase in decohesion gap with clear view of circumferential internal crack. The fracture surface study showed the presence of large irregular graphite particles along the crack path (Fig. 10). Such embedded irregular graphite particles have a significant influence on primary crack propagation and final fracture of the SGI components. Larger submerged defects could initiate secondary cracks and form crack branch, indicating complex nature of crack propagation in SGI microstructure.

Fatigue crack propagation test

The SEM results of short and long crack studies in FCP tests are presented in Fig. 11 and 12 respectively. For short crack, FCP test was stopped after 61,000 cycles; whereas for long crack, test was stopped after 97,000 cycles. Usually, multiple crack initiations were observed at the notch (Fig. 11: a) and Fig. 12: a), d)) but only one crack further propagated, other cracks were arrested within the ferrite matrix or at the graphite nodule. Dominant growth of the main crack gave insight on the fatigue crack propagation mechanism without influence of other cracks. The primary crack propagated towards neighboring graphite nodules and connecting most of them to the crack path. Such crack growth led to a zigzag crack path which was also reported in previous works.[2,7,8]

Fig. 10 SEM images of short intermediate fatigue crack (R = 0.1, $\triangle K_{Start}$ = 13 MPa√m, a = 0.75 mm, $\triangle K$ = 27 MPa√m)

Fig. 11 SEM images of long intermediate fatigue crack (R = 0.1, $\triangle K_{Start}$ = 13 MPa√m, a = 1.67 mm, $\triangle K$ = 35 MPa√m)

Graphite/ferrite interface decohesion is considered as one of the frequent damage mechanism in SGI iron, which was clearly visualised in many occasions. Partial decohesion of spheroidal graphite particles took shorter path toward next graphite nodule (Fig. 11: b), e), f)). Such partial decohesion seemed to provide crack tip blunting effect that stopped further crack propagation for a short time. In case of multiple cracks initiation at the notch, some cracks were completely arrested at the graphite nodule, which highlighted graphite nodule as

possible crack arrester. In Fig. 11: h) similar phenomenon was observed, where the crack tip just reached a graphite nodule that stopped crack propagation. After additional cycles, the arrested crack further propagated into the ferrite matrix until it reached next graphite nodule. This type of graphite decohesion left partially embedded graphite nodule on fracture surface. Many such partially debonded types of graphite nodules were observed along the crack paths in Fig. 11 and 12.

Even in most cases crack propagated by connecting graphite nodules, sometimes crack simply passed through the ferrite matrix in between graphite nodules (Fig. 11 and 12). It was believed that such crack growth was governed by submerged graphite nodules unexposed to the surface. In Fig. 12: c an illustration of such case was captured. At the crack tip area that lied between two surface graphite nodules, a graphite nodule was slightly exposed just below the crack path supporting that such crack growth was influenced by the submerged graphite nodule. So, the random distributions of the submerged graphite nodules were likely to influence fatigue crack growth.

Fig. 12 SEM studies of graphite particles along the crack path of completely fractured C(T) specimen (R = 0.1, $\triangle K_{Start}$ = 13 MPa√m)

The compacted and irregular graphite particles presented in the microstructure behaved differently than spheroidal graphite nodules. As shown in Fig. 11: c) and Fig. 13: d), the compacted graphite particles present in the crack path were damaged and the crack passed through narrow section of the compacted graphite. Cracks branching were observed around graphite nodules. When multiple graphite nodules were present near the crack, the crack tended to branch (Fig. 12: b), e)). Crack branching observed was not always from the main crack; instead, graphite nodule near the crack tip was likely to debond and initiate a microcrack, which grew toward the main crack and connect with it to form a crack branch similar to that observed in Fig. 12: e). At the stable propagation region, steady crack growth connected graphite nodules. The plastic zone size in this region was smaller, so only few graphite nodules near the crack tip were influenced by crack tip stress intensification. As the crack size increased to the unstable region, the plastic zone became larger and most of the graphite nodules around were influenced as shown in Fig. 12: f). The graphites nodules were mostly debonded from the matrix and many secondary cracks were nucleated at the crack tip region. At this region, crack propagation was by coalescence of nucleated voids and secondary cracks, and its linkup with the primary crack.

The role of graphite nodules on the FCP mechanisms at different fatigue region is illustrated in Fig. 13. It presents the state of graphite nodules along the crack path of the completely fractured C(T) specimen. Two

distinct crack regions; stable crack propagation region and unstable crack propagation region were observed. The stable crack path was characterised by a steady crack surface as compared to the unstable crack propagation region characterised by a more random crack path. Fig. 13: a) shows partially decohesion of graphite nodule at the crack initiation site, which showed graphite nodule could assist crack initiation. The compacted graphite particles were damaged when the crack passed through them (13: b) and d)). Secondary cracks and crack branching explained in the above section is evident in Fig. 13: c) as well. Fig. 13: e) – h) shows graphite particles at and around the crack path in the unstable region. Sign of graphite nodule decohesion with graphite void growth due to large plastic deformation was clearly seen. These voids could coalesce by fracture of the ferrite matrix to form a microcrack. In the beginning, the graphite nodule acted like defect that can assist during crack initiation, in the stable crack propagation region it gave crack tip blunting effect by partial decohesion that stopped crack growth for a while and finally in the unstable region it acted like a void in the matrix that gradually grew in size with continuous plastic deformation of the ferrite matrix.

Fig. 13 Fracture surface and magnified SEM images of fracture surface at different regions (R = 0.1, $\triangle K_{Start}$ = 13 MPa$\sqrt{m}$)

Fig. 14 shows the fracture surface of the whole CT specimen with enlarged views in different zones. The fracture surface was described by partially disintegrated graphite nodules and empty graphite voids. Some secondary cracks were also detected in the ferrite matrix between graphite nodules. Fracture surface in the stable region exposed partially disintegrated graphite nodules with a narrow decohesion gap. The size of the empty graphite pockets was similar to the graphite nodule size, which suggested slow decohesion of graphite nodule with less plastic deformation. The decohesion gap gradually increased at the transition region where fracture surface was partly similar to the stable region and partly similar to the unstable region. Fracture surface at the unstable region was characterised by the complete disintegration of graphite nodules due to large void growth. The size of the graphite pockets was larger than the graphite nodule size illustrating large plastic flow of the ferrite matrix. Due to higher plastic deformation, reduction of thickness and elongation of the specimen could be clearly seen in the unstable region. The fracture study results were similar to that reported in literature by Fernandino et al.[36] and correlated with the tensile fracture surface.

DISCUSSION

According to the experimental results observed, the role of the graphite nodules on fatigue damage depends on the graphite form and could be different at different stage. The fatigue damage mechanisms are explained in

three fatigue stages, namely; crack initiation and tiny crack growth (stage I), stable crack growth (stage II) and rapid unstable crack growth (stage III).

Stage I – Fatigue crack initiation and tiny crack growth

Based on fatigue damage initiation theory, crack initiation under cyclic load is due to the formation of irreversible dislocations, its accumulation to develop slip steps and slip bands, which act as possible crack initiation sites.[32] In SGI, the presence of different forms of graphite nodules and casting defects cause inhomogeneous strain and stress distribution. Strain localisation was reported around graphite nodules that led to microcrack initiation.[17] Such strain localisation was highly dependent on the shape and size of the graphite nodule and defect. Roundness shape factor was evaluated for all the graphite nodules that showed some sort of damage (Fig. 6 and 7). The graphite nodules showed two distinct damage initiation mechanisms. Even most of the graphite nodules were spheroidal; a small fraction was compacted and irregular with lower RSF values. Mostly, the graphite nodules with RSF less than 0.5 and perpendicular to the loading direction initiated fatigue microcracks. Most of the spheroidal graphite nodules were still intact at the time of early crack initiation from degenerated graphite nodules. Greno et al.[5] had reported that the graphite nodules were not perfect spheres of flat surface; instead, the graphite/matrix interface was extremely irregular, which could also be observed in the fracture surface (Fig. 14). This irregular interface provided stronger bonding to resist graphite-ferrite decohesion.

The compacted graphite particles with RSF less than 0.5 showed internal cracking that further grew into the ferrite matrix to form microcracks. This type of graphite growth was mostly along the a-direction (basal plane) in the hcp lattice structure of the graphene layer. It was reported that the bonding between the basal planes or graphene layers were weak during graphite growth.[33] This weak bonding and soft nature of the graphite nucleated from melt might be weaker than the interface bond resulting into graphite internal cracking. The elongated shape of these graphite particles developed higher stress concentration than spheroidal graphite nodules that contributed to crack growth into the ferrite matrix (Fig. 6, 7 and 8).

The damage of spheroidal graphite nodules was different from that of compacted graphite particles. Most of the averaged sized graphite nodules were not affected during the early crack initiation stage as the rough graphite/matrix bonding was strong enough to resist stress localisation around the spheroidal graphite nodules. Larger spheroidal graphite noduless showed internal cracking into ring and core (Fig. 6, 7 and 8). These fully grown graphite nodules corresponded to graphite nucleation and growth from melt (C_M), growth from eutectic solidification (C_E), growth due to reduced C solubility in austenite grain (C_A) and growth by eutectoid

transformation into ferrite (C_F), which caused property variation within the graphite nodule.[7,34,35] Other smaller graphite nodules growths were usually due to one of the above mention growth process or by combination. It was reported that the lower resistance corresponded to the interface ($C_M + C_E$) versus ($C_A + C_F$), where internal damage of the graphite nodule was usually observed.[7,22] At the early crack initiation stage without large crack tip stress field, ($C_M + C_E$) versus ($C_A + C_F$) interface was weaker than the graphite/ferrite interface, initiating internal damage of the graphite nodules. The spheroidal graphite damage observed was circumferential in SGI, which was supported by the previous work[33] showing spheroidal graphite growth along the circumference.

Casting defects were always considered as one of the main crack initiation point in all cast metals.[19,20] Defects like shrinkage porosity acted as voids in the metal matrix that raised local stress concentration around it. In the investigated high Si SGI, shrinkage porosities of size smaller or comparable to graphite nodule were observed. These shrinkage porosities initiated cracks at similar load cycles as most of the compacted graphite particles. So, it can be concluded that the shrinkage porosity defect comparable or smaller than graphite nodule size behaved similar to compacted type graphite from the fatigue crack initiation point. However, the presence of larger casting defects would have a major influence on the crack initiation and propagation behaviour.

Stage II – Stable fatigue crack growth

After initiation of the fatigue crack and growth to microcrack, crack growth and its direction was influenced by the loading direction. On a macro scale, the crack would have propagated in a direction perpendicular to the loading direction. But in micro scale, the crack was likely to change its direction due to the random distribution of graphite nodules. This is the region where most of the fatigue crack growth laws, including Paris' law, are valid.

Spheroidal graphite nodules were the common graphite morphology in SGI. So, partial decohesion of the spheroidal graphite nodules along the crack profile was the most frequent damage mechanism at this stage. During the stable crack propagation, the property gradient within graphite nodules did not play a significant role due to the presence of higher stress concentration at the crack tip. This stress concentration resulted into decohesion of graphite/ferrite interface prior to internal cracking of graphite nodule. The reported roles of spheroidal graphite as possible crack arrester and crack tip blunting effect were also highlighted in this region.[2,6,8] As the crack tip reached near a spheroidal graphite, higher local stress in front of the crack tip exceeded the fracture stress of the graphite/ferrite interface (Fig. 11 and 12). This led to decohesion of the interface, reducing stress concentration and inducing crack tip blunting effect that stopped the crack growth for a short time. In some occasions, cracks completely stopped further propagation at such graphite nodules

demonstrating spheroidal graphite nodules as possible crack arresters. The peculiar shape of spheroidal graphite nodules could significantly reduce crack tip stresses and provide higher fatigue resistance to SGI compared to other cast irons.

In the presence of multiple graphite nodules in front of the crack tip, the crack might grow toward one graphite nodule until microcrack reached certain length adopting necessary geometry to cause load shielding effect, ultimately stopping further growth. The primary crack would then grow towards another graphite nodule forming a crack branch. Another possibility of crack branching was from the graphite nodules with microcracks near the primary crack. Increase in the primary crack length raised the value of ΔK in the vicinity of the crack tip that caused graphite decohesion and microcrack initiation at larger distance. The initiated microcracks grew towards the primary crack to from a crack branch. Similar possibilities were also reported in earlier work by Greno et at.[5]

Propagation of the fatigue crack in the ferrite matrix between graphite nodules was reported on previous cases[2,6,8] and also observed in this study (Fig. 11). Most of the crack propagation study was limited to surface microstructure observation but the graphite nodules were randomly distributed all over the specimen. These randomly distributed graphite nodules created inhomogeneous stress distribution in 3D field. So, the crack propagation in SGI was also influenced by the submerged graphite nodule distribution. It was observed in an occasion (Fig. 12 c)) that the crack propagation in the ferrite matrix was influenced by the submerged graphite nodules.

Compacted and irregular graphite particles played crucial role to initiate microcrack. In the stable crack propagation region, such compacted and irregular graphite particles behaved slightly different than spheroidal graphite nodules. Because of their elongated shape, the crack tip blunting effect provided by spheroidal graphite nodule was not well realized in degenerated graphite nodules. In this study, it was observed that the crack advanced by fracture of the graphite nodule at the narrow section if the graphite nodule was at acute angle to the loading direction (perpendicular to the crack growth direction), whereas if the compacted graphite nodule was perpendicular or at larger angle (parallel to the crack growth direction), the crack propagated by decohesion of the graphite nodule that followed the matrix cracking on the other end of the compacted or irregular graphite particle. So, the role of the degenerated graphite nodules and crack propagation through them depends on the orientation and shape of the graphite nodule.

Stage III - Rapid unstable crack growth

Further growth of crack into the unstable region led to an increased ΔK on the remaining section by redistribution of the applied load, so that the crack tip stress field extended to a larger area. The matrix alone was no longer able to sustain the load causing large plastic flow of the matrix that caused decohesion of graphite nodules creating large voids. Here, the graphite nodules acted like void defects after decohesion and initiated multiple microcracks. Then the final failure was by growth and coalescence of the graphite voids and initiated microcracks causing unstable crack propagation. The failure mechanism and the role of graphite nodule at this stage showed similarities to rapid fracture in tensile test.

CONCLUSION

Fatigue damage mechanisms in high Si SGI were investigated based on the FCI and FCP tests. On the basis of the experimental results, following conclusions can be made:

- Cracks initiation in high Si SGI was mostly from degenerated graphite nodules and casting defects. Degenerated graphite nodules with RSF less than 0.5 initiated cracks either by internal cracking of the graphite nodules followed by cracks initiation into the matrix; or by graphite nodules decohesion followed by cracks initiation; or by combination of these mechanisms. However, all the graphite particles with RSF values less than 0.5 did not initiated cracks as the initiation was also affected by orientation and shape of the graphite particles. Graphite nodules with RSF higher than 0.5 mostly showed graphite nodules decohesion, spheroidal graphite nodules with RSF higher than 0.9 in specific did not initiated early cracks. Instead, the larger spheroidal graphite nodules showed circumferential internal cracking and graphite/ferrite decohesion. Shrinkage porosities smaller or size comparable to that of the graphite nodules had similar crack initiation effect as degenerated graphite nodules.
- Spheroidal graphite/ferrite matrix interface decohesion was a frequently observed damage mechanism for crack propagation. Decohesion of spheroidal graphite nodules from the ferrite matrix provided crack tip blunting effect that stopped propagation for few additional load cycles. However, the crack tip blunting effect and crack growth depends on RSF. Spheroidal graphite nodules with higher RSF showed clear decohesion, whereas degenerated graphites with lower RSF were either fractured (perpendicular to the crack growth direction) or decohesion followed by the matrix cracking (parallel to the crack growth direction). Crack often formed branches when a crack initiated from the graphite nodules near the crack tip and propagated towards the primary crack, or in the presence of multiple graphite nodules in front of the crack tip.

- The graphite nodules in the unstable region behaved like voids in the ferrite after decohesion. Irrespective of the RSF values, these voids grew due to plastic flow of the ferrite matrix and coalescence to form microcracks. Rapid propagation of the main crack by connecting initiated microcracks led to final fracture of the specimen.

This study provided comprehensive understanding of fatigue damage micromechanisms in SGI. Graphite nodules being important phase in SGI microstructure, the roles played by graphite nodules on damage mechanism is investigated based on the RSF. It was shown that graphite morphology plays vital role in fatigue damage micromechanism of SGI and the role could be different at different fatigue stage. The damage mechanism understanding comes handy in an attempt to optimize SGI microstructure for better fatigue behavior and would be very useful in an effort to model SGI microstructure for failure prediction.

ACKNOWLEDGEMENT

This work was supported by the Singapore Ministry of Education (MOE) Academic Research Funding (AcRF) Tier 1 Grand RG26/12. The authors wish to acknowledge financial support by JASSO for TiROP exchange program in Tokyo Institute of Technology and CompCAST project (2010280) funded by the Knowledge Foundation in Sweden.

REFERENCE

1 Labrecque C, Gagné M (1998) Review ductile iron: fifty years of continuous development. *Can. Metall. Quart*. **37**: 343-378.

2 Iacoviello F, Cocco VD, Cavallini M (2010) Ductile cast irons: microstructure influence on fatigue crack propagation resistance. *Frattura ed Integritá Strutturale*. 3-16.

3 Gonzaga RA (2013) Influence of ferrite and pearlite content on mechanical properties of ductile cast irons. *Mater. Sci. and Eng., A*. **567**: 1-8.

4 Jeckins LR, Forrest RD (1993) Properties and selection: Iron, Steel and High performance alloys. *ASM Handbook*. 10 edn. American Society for Metals, Metals Park, Ohio,, 3-56.

5 Greno GL, Otegui JL, Boeri RE (1999) Mechanisms of fatigue crack growth in Austempered Ductile Iron. *Int. J. Fatigue*. **21**: 35-43.

6 Iacoviello F, Di Cocco V, Rossi A, Cavallini M (2013) Pearlitic ductile cast iron: damaging micromechanisms at crack tip. *Frattura ed Integrita Strutturale*. **25**: 102-108.

7 Di Cocco V, Iacoviello F, Ross A, cavallini M, Natali S (2013) Graphite nodules and fatigue crack propagation micromechanisms in a ferritic ductile cast iron. *Fatigue Fract. Engng Mater. Struct.* **36**: 893.

8 Di Cocco V, Iacoviello F, Rossi A, Iacoviello D (2014) Macro and microscopical approach to the damaging micromechanisms analysis in a ferritic ductile cast iron. *Theor. Appl. Fract. Mec*. **69**: 26-33.

9 Dong MJ, Prioul C, François D (1997) Damage effect on the fracture toughness of nodular cast iron: Part I. Damage characterization and plastic flow stress modeling. *Metall. Mat. Trans., A*. **28**: 2245-2254.

10 Tokaji K, Ogawa T, Shamoto K (1994) Fatigue crack propagation in spheroidal-graphite cast irons with different microstructures. *Int. J. Fatigue*. **16**: 344-350.

11 Zambrano HR, Härkegärd G, Stärk KF (2012) Fracture toughness and growth of short and long fatigue cracks in ductile cast iron EN-GJS-400-18-LT. *Fatigue Fract. Engng Mater. Struct.* **35**: 374-388.

12 Martínez RA (2010) Fracture surfaces and the associated failure mechanisms in ductile iron with different matrices and load bearing. *Eng. Fract. Mech*. **77**: 2749-2762.

13 Iacoviello F, Di Cocco V, Cavallini M (2016) Fatigue crack propagation and overload damaging micromechanisms in a ferritic-pearlitic ductile cast iron. *Fatigue Fract. Engng Mater. Struct.* **39**: 999.

14 Marrow TJ, Çetinel H, Al-Zalmah M, MacDonald S, Withers PJ, Walton J (2000) Short fatigue cracks in austempered ductile cast iron (ADI). *Fatigue Fract. Engng Mater. Struct.* **23**: 425-434.

15 Marrow TJ, Çetinel H, Al-Zalmah M, MacDonald S, Withers PJ, Walton J (2002) Fatigue crack nuclei in austempered ductile cast iron. *Fatigue Fract. Engng Mater. Struct.* **25**: 635.

16 Griswold Jr FD, Stephens RI (1987) Comparison of fatigue properties of nodular cast iron production and Y-block castings. *Int. J. Fatigue*.**9**: 3-10.

17 Kasvayee KA, Ghassemali E, Jarfors AEW (2015) Micro-Crack initiation in high-silicon cast iron during tension loadin. *TMS2015*, 947-953.

18 Kasvayee KA, Salomonsson K, Ghassemali E, Jarfors AEW (2016) Microstructural strain distribution in ductile iron; comparison between finite element simulation and digital image correlation measurements. *Mater. Sci. and Eng., A*. **655**: 27-35.

19 Shirani M, Härkegård G (2011) Casting defects and fatigue behaviour of ductile cast iron for wind turbine components: A comprehensive study *Materialwissenschaft und Werkstofftechnik*. **42**: 1059-1074.

20 Endo M, Yanase K (2014) Effects of small defects, matrix structures and loading conditions on the fatigue strength of ductile cast irons. *Theor. Appl. Fract. Mec*. **69**: 34-43.

21 Iacoviello F, Di Cocco V, Rossi A, Cavallini M (2015) Fatigue crack tip damaging micromechanisms in pearlitic ductile cast irons. *Fatigue Fract. Engng Mater. Struct.* **38**: 238-245.

22 Cocco VD, Iacoviello F, Rossi A, Cavallini M, Natali S, Ecarla F (2013) Mechanical properties gradient in graphite nodules: influence on ferritic DCI damaging micromechanisms. *Acta Fract.* Roma, Italia, 222–230.

23 Matsushita T, Ghassemali E, Saro AG, Elmquist L, Jarfors AEW (2015) On Thermal Expansion and Density of CGI and SCI Cast Irons. *Metals*. **5**: 1000-1019.

24 Alhussein A, Risbet M, Bastien A, Chobaut JP, Balloy D, Favergeon J (2014) Influence of silicon and addition elements on the mechanical behavior of ferritic ductile cast iron. *Mater. Sci. and Eng., A*. **605**: 222-228.

25 Muhmond HM, Fredriksson H (2014) Graphite Growth Morphologies in Cast Iron. *Mater. Sci. forum*. **790**: 458-463.

26 Muhmond HM, Fredriksson H (2014) Relationship Between the Trace Elements and Graphite Growth Morphologies in Cast Iron. *Metall. Mat. Trans., A*. **45**: 6187-6199.

27 Double DD, Hellawell A (1995) The nucleation and growth of graphite—the modification of cast iron. *Acta Metall. Mater*. **43**: 2435-2442.

28 Skaland T (2003) Ductile iron shrinkage control through graphite nucleation and growth. *Int. J. Cast Met. Res.* **16**: 11.

29 Igarashi Y, Okada S (1998) Observation and Analysis of the Nucleus of Spheroidal Graphite in Magnesium Treated Ductile Iron. *Int. J. Cast Met. Res.* **11**: 83-88.

30 Čanžar P, Tonković Z, Kodvanj J (2012) Microstructure influence on fatigue behaviour of nodular cast iron. *Mater. Sci. and Eng., A*. **556**: 88-99.

31 Sujakhu S, Castagne S, Sakaguchi M, Kasvayee KA, Ghassemali E, Jarfors AEW, Wang W (2017) Micromechanisms Investigation on Fatigue Crack Initiation and Propagation in High Silicon Spheroidal Graphite Cast Iron. *Proceeding of 8th Low Cycle Fatigue Conference*, June 27 – 29, Dresden, Germany.

32 Bhat S, Patibandla R (2011) Metal Fatigue and Basic Theoritical Models: A Review. *Alloy Steel - Properties and Use,* 203-236.

33 Muhmond HM (2014) On the Inoculation and Graphite Morphologies of Cast Iron. Ph.D. dissertation, *Dept. Mat. Sci. Eng*. Royal Institute of Technology, Stockholm, Sweden.

34 Pradhan SK, Nayak BB, Sahay SS, Mishra BK (2009) Mechanical properties of graphite flakes and spherulites measured by nanoindentation. *Carbon*. **47**: 2290-2292.

35 Randall NX, Vandamme M, Ulm F-J (2009) Nanoindentation analysis as a two-dimensional tool for mapping the mechanical properties of complex surfaces. *J. Mater. Res*. **24**: 11.

36 Fernandino DO, Boeri R (2015) Study of the fracture of ferritic ductile cast iron under different loading conditions. *Fatigue Fract. Engng Mater. Struct.* **38**: 610-620.

Figures

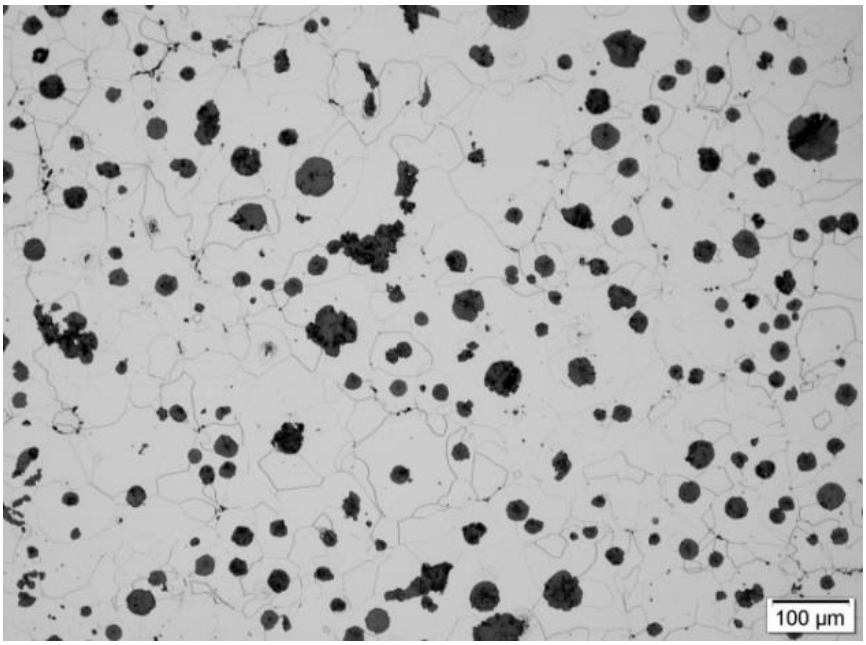

Fig. 14 Microstructure of EN-GJS-500-14

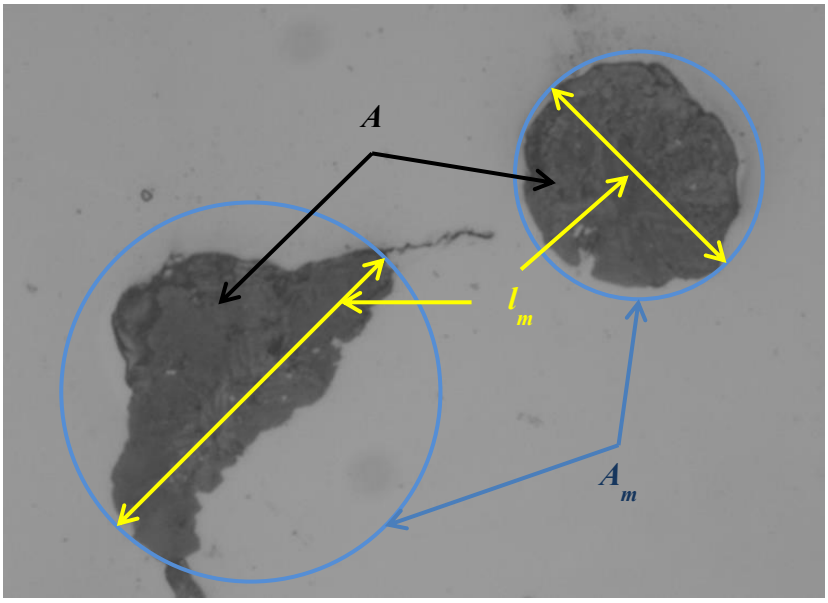

Fig. 15 Roundness shape factor definition

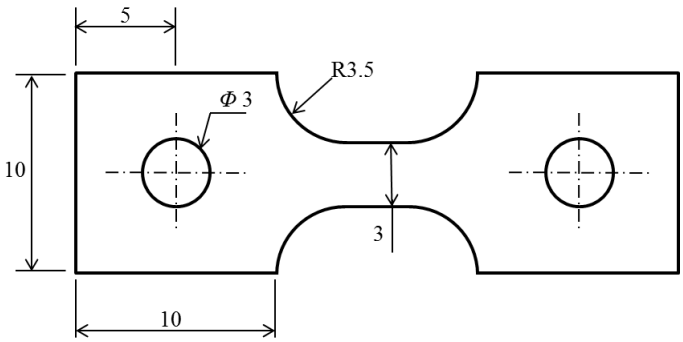

Fig. 16 Miniature pin-loaded tensile specimen for crack initiation test (all dimensions in mm)

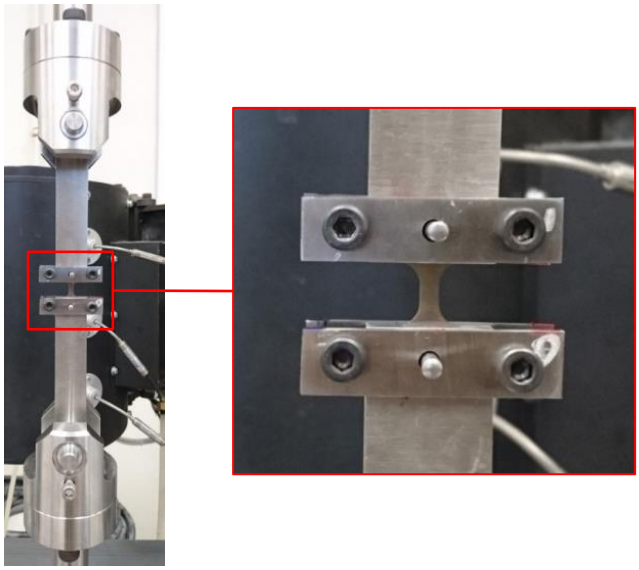

Fig. 17 Clamping fixture design for crack initiation test

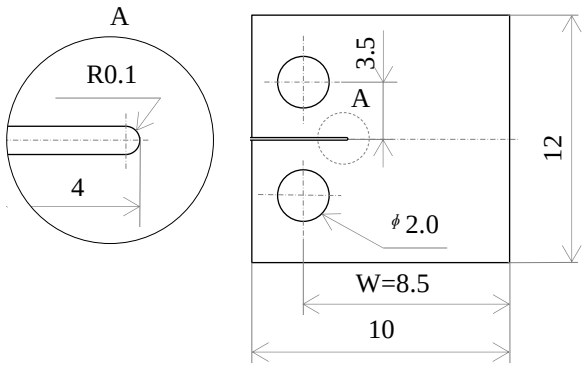

Fig. 18 Miniature C(T) specimen design for crack propagation test (all dimensions in mm)

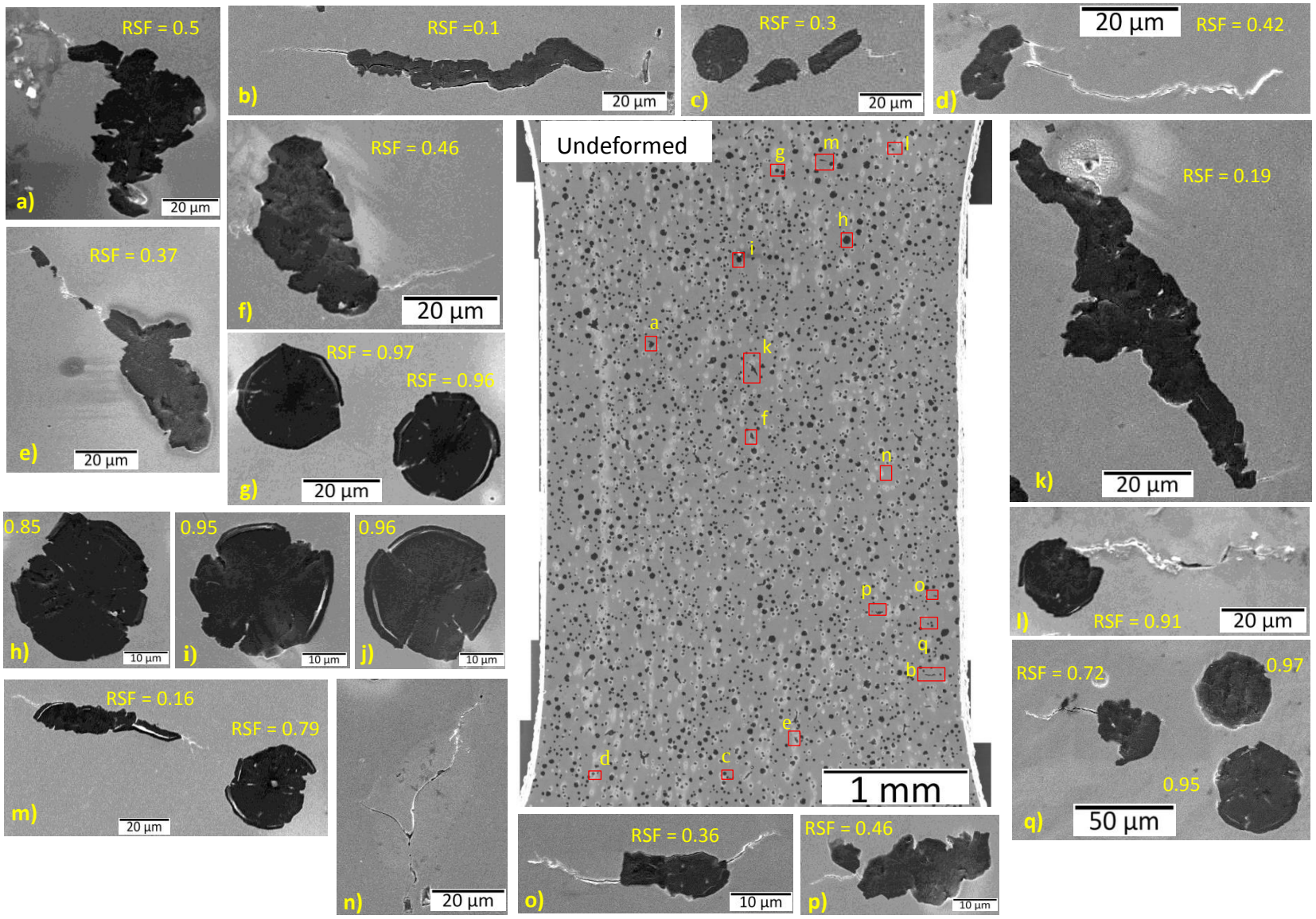

Fig. 19 Fatigue damage initiations on face 1 of the miniature FCI specimen(R = 0.1, S_{max} = 350 MPa, N = 390,000 cycles)

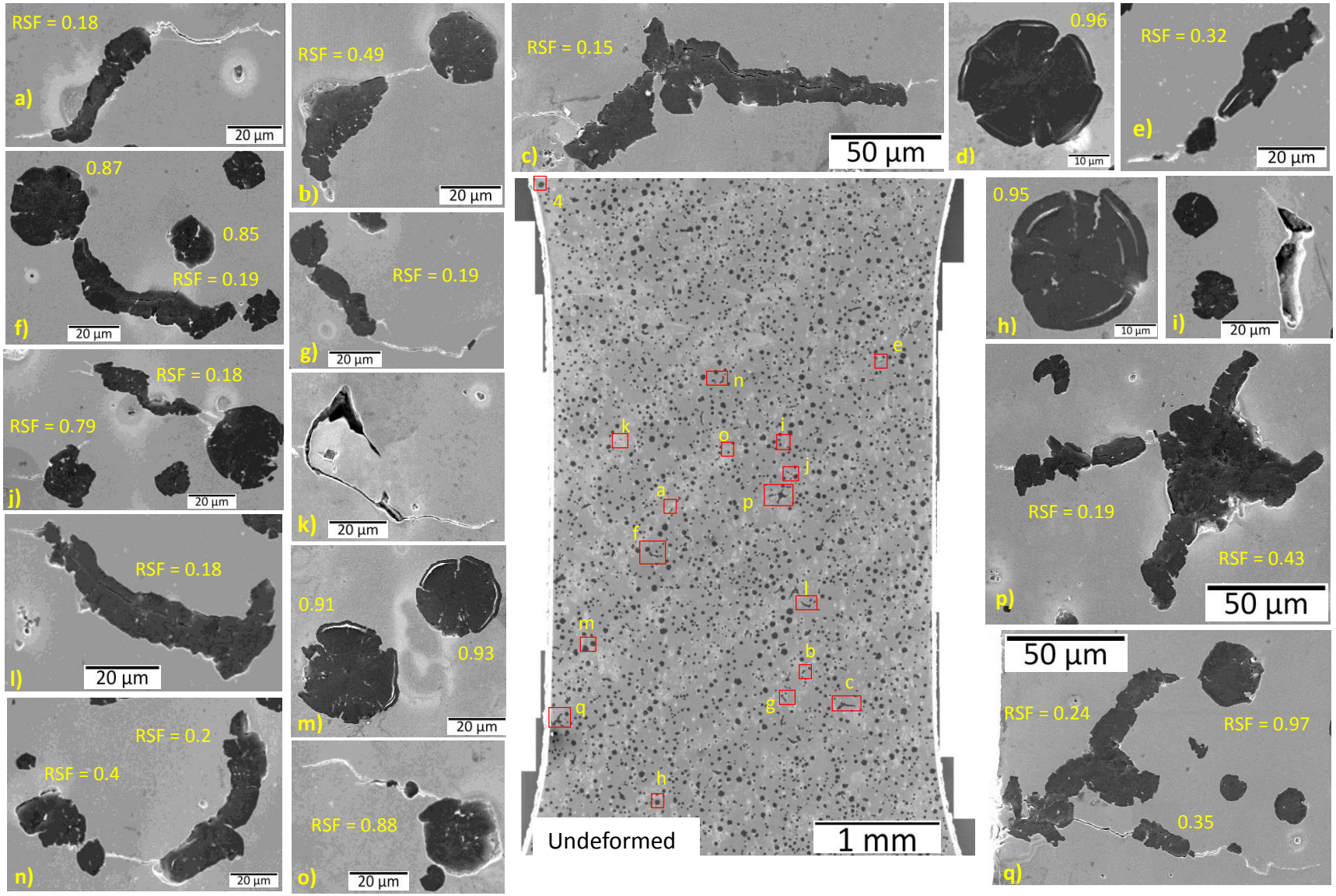

Fig. 20 Fatigue damage initiations on face 2 of the miniature FCI specimen(R = 0.1, S_{max} = 350 MPa, N = 390,000 cycles)

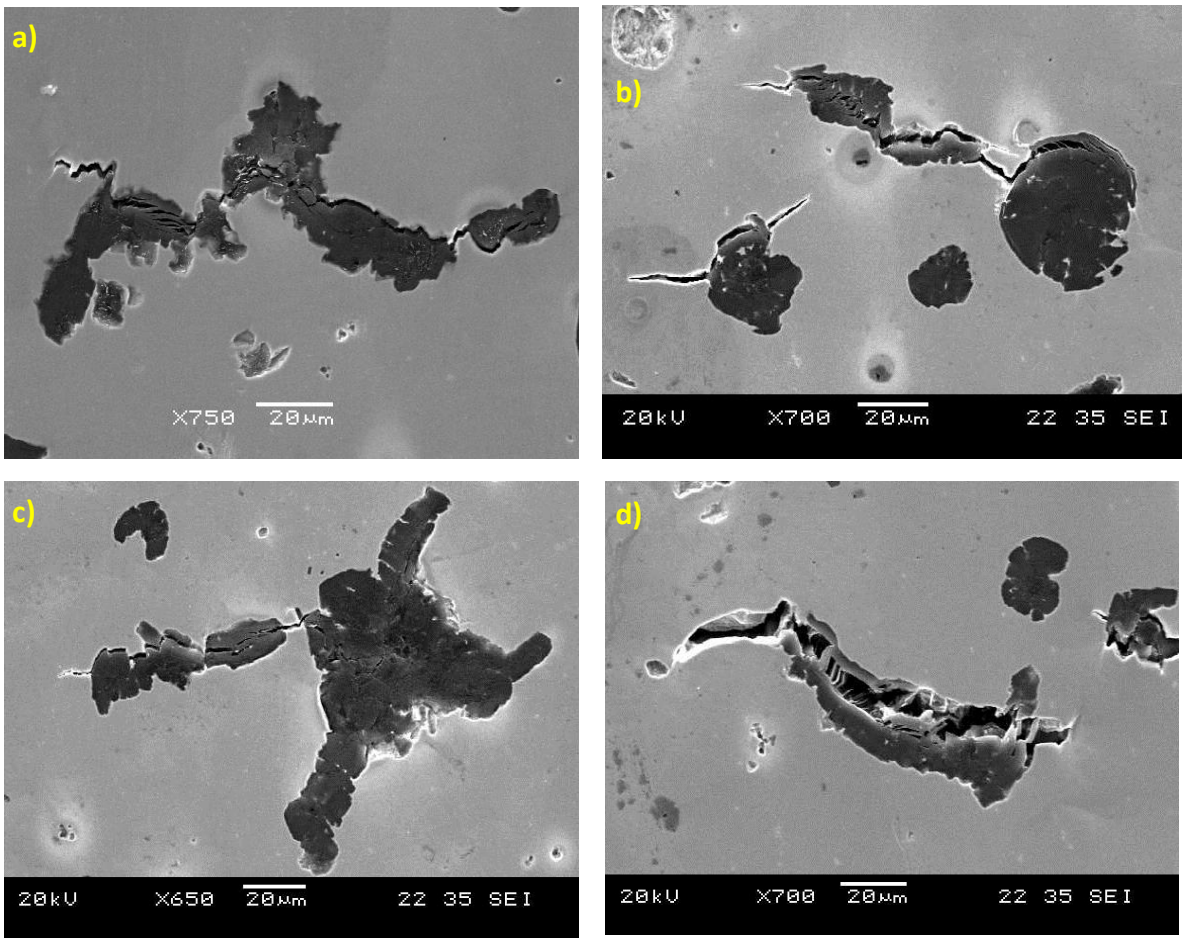

Fig. 21 Degenerated graphites and initiated cracks after final failure of the specimen (R = 0.1, S_{max} = 350 MPa, N_f = 474047)

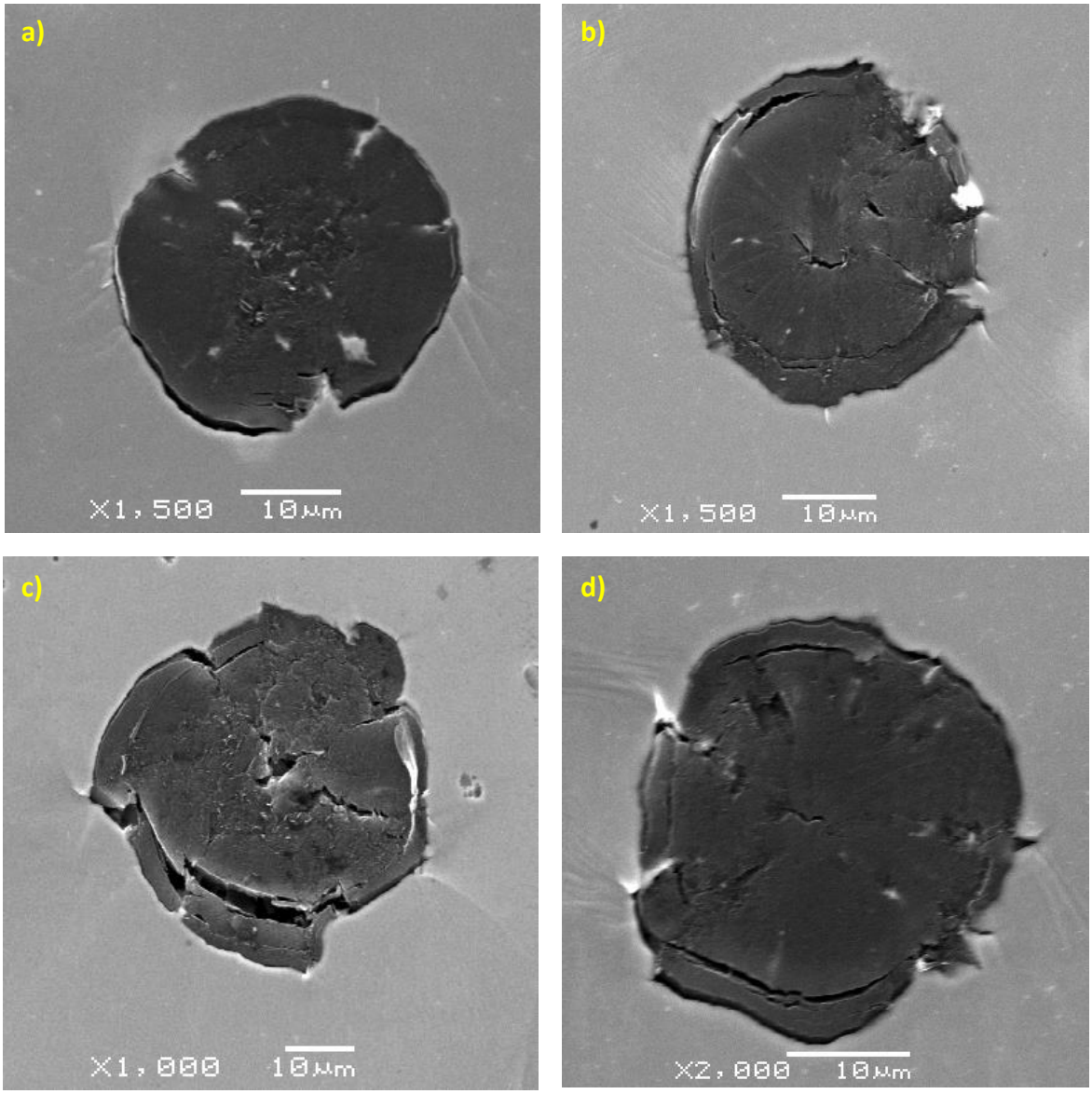

Fig. 22 Spheroidal graphite nodules after final failure of the specimen (R = 0.1, S_{max} = 350 MPa, N_f = 474047)

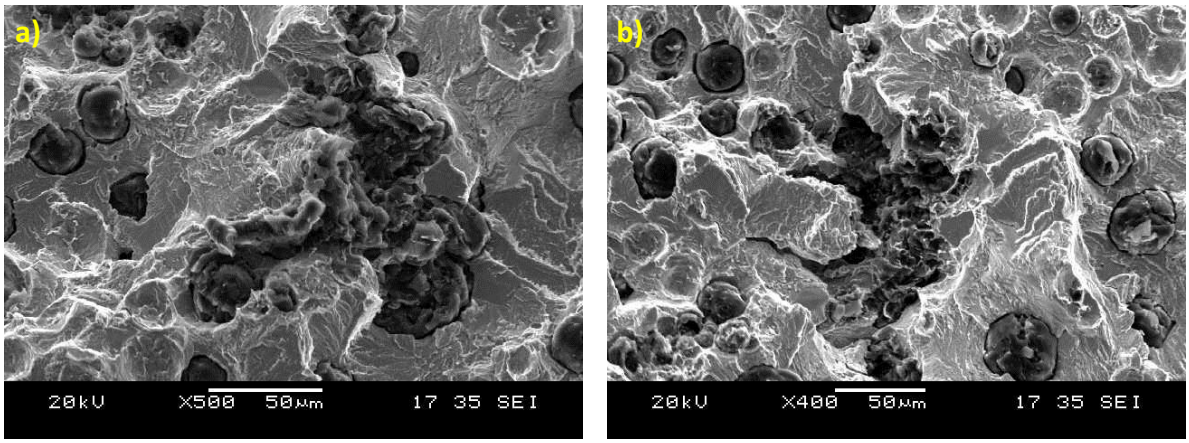

Fig. 23 Large irregular graphites on the fracture surface of the specimen (R = 0.1, S_{max} = 350 MPa, N_f = 474047)

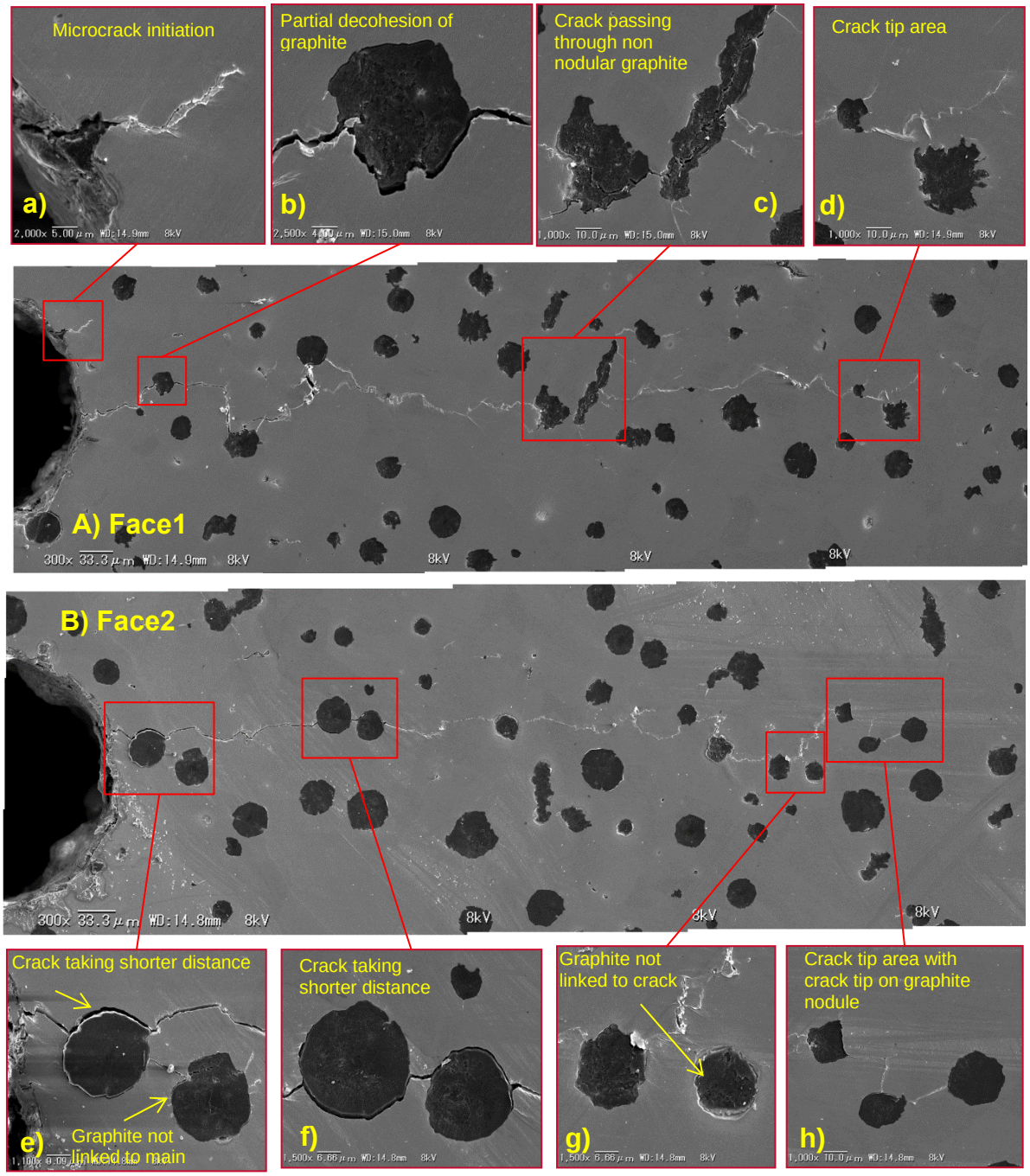

Fig. 24 SEM images of short intermediate fatigue crack (R = 0.1, ΔK_{Start} = 13 MPa√m, a = 0.75 mm, ΔK = 27 MPa√m)

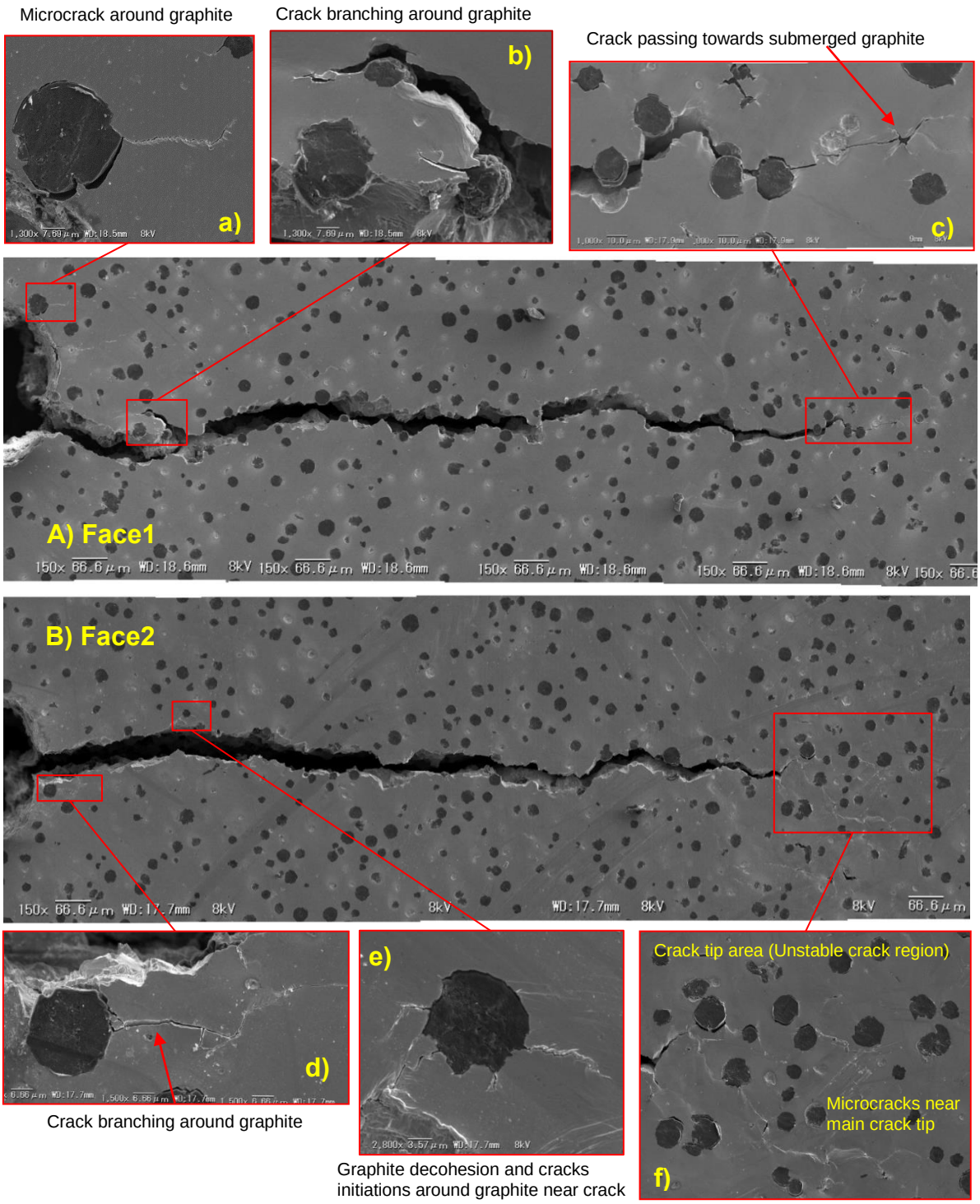

Fig. 25 SEM images of long intermediate fatigue crack (R = 0.1, ΔK_{Start} = 13 MPa√m, a = 1.67 mm, ΔK = 35 MPa√m)

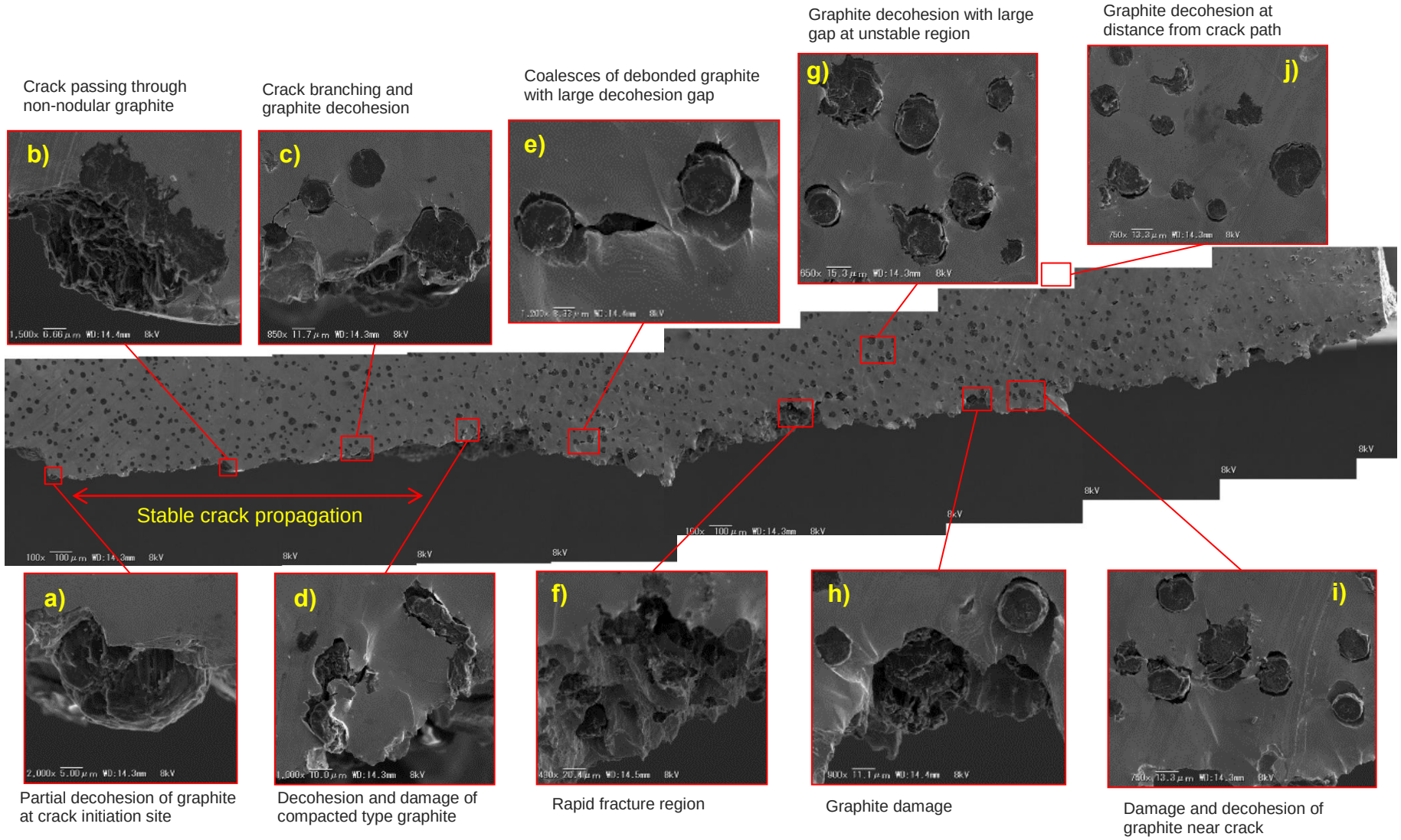

Fig. 26 SEM studies of graphite particles along the crack path of completely fractured C(T) specimen (R = 0.1, ΔK_{Start} = 13 MPa$\sqrt{m}$)

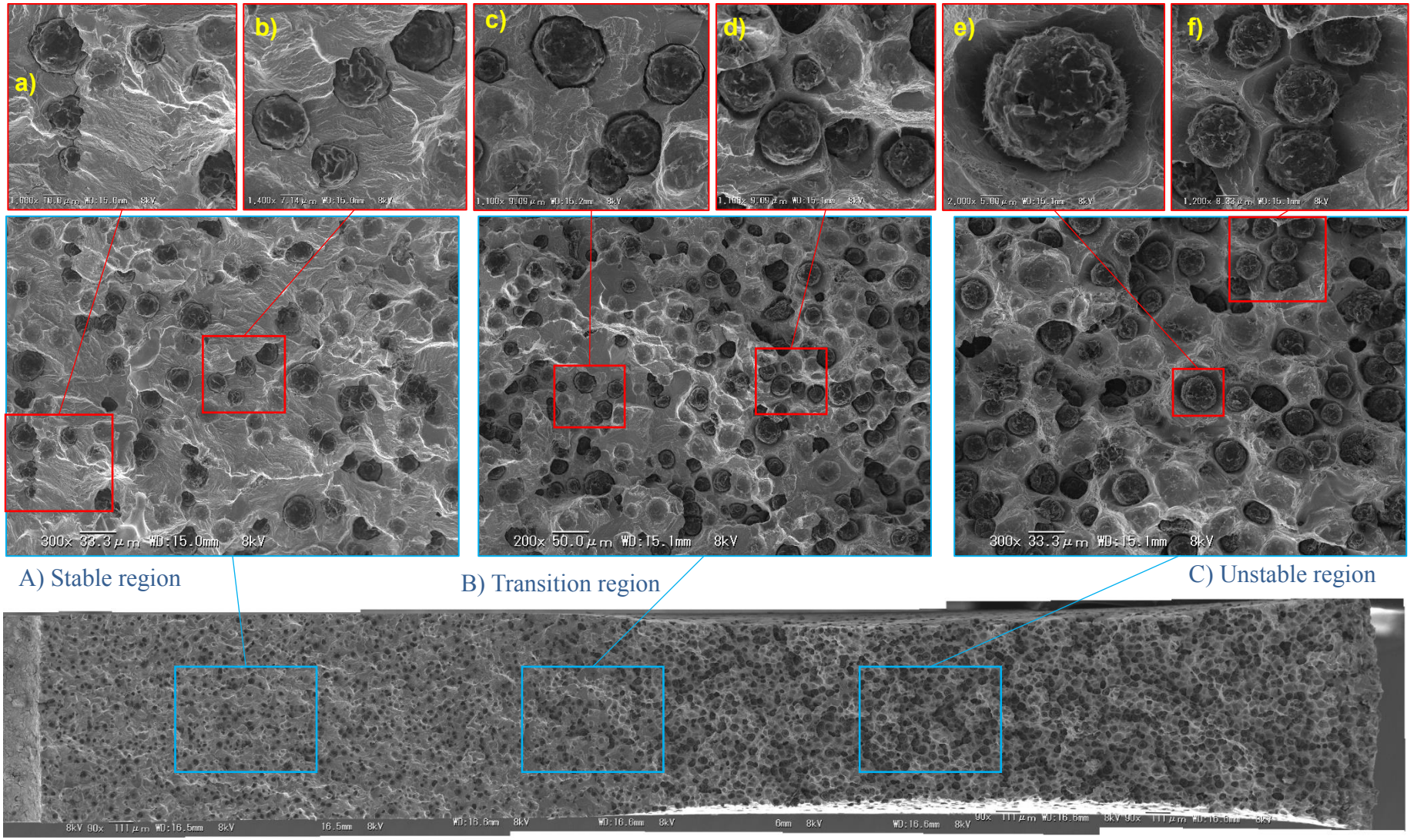

Fig. 27 Fracture surface and magnified SEM images of fracture surface at different regions (R = 0.1, ΔK_{Start} = 13 MPa√m)

Tables

Table 1 Chemical composition of EN-GJS-500-14 (%wt.)

C	Si	Cu	Mn	S	Mg	Sb	Fe	C_{eq}*
3.2	3.71	0.053	0.182	0.006	0.042	0.0058	92.5	4.15

* C_{eq} is carbon equivalent value that represents the equivalent percentage of carbon considering the effect of other alloying elements. Carbon equivalent mostly depends on C, Si and P content and can be calculated using $C_{eq} = C\% + 1/3(Si\% + P\%)$.

Table 2 Tensile properties of EN-GJS-500-14 (50 mm thick plate)

Young's modulus (GPa)	Yield Strength (MPa)	UTS (MPa)	Elongation to fracture (%)
170 ± 1	410 ± 9	511 ± 6	17 ± 6

Table 3 Microstructure characterization of EN-GJS-500-14 cast

Avg. Diameter (μm)	Nodularity by area (%)	Nodule count (per mm^2)	Pearlite fraction (%)	Graphite fraction (%)
27 ± 8	74 ± 3	122 ± 36	1 ± 1	9 ± 0.5